1.55 µm DFB laser monolithically integrated with amplifier array

Lianping Hou,* John H. Marsh

School of Engineering, University of Glasgow, Glasgow, G12 8LT, U.K.
** Corresponding author:lianping.hou@glasgow.ac.uk*

We present a laterally-coupled 1.55 µm distributed feedback laser monolithically integrated with multistage multi-mode interferences and semiconductor optical amplifiers, using low bias currents and providing an output power of ~100 mW with a quasi-single spatial mode far field pattern and low divergence angle of 3.5° in the horizontal direction. The fabrication techniques are based on side-wall gratings and quantum-well intermixing and offer a simple, flexible and low cost alternative to conventional methods.

OCIS codes: 140.3490, 250.5980, 130.3120

High power, single-frequency and quasi-single spatial-mode semiconductor lasers operating at wavelengths around 1.55 µm are essential components in many applications such as Raman pumps for fiber communication systems, spectroscopy, remote sensing, free-space communications, eye-safe laser based radar (LIDAR), and wavelength conversion in nonlinear materials [1]. Semiconductor laser arrays are advantageous over single element systems for high power applications as the total power output of the device can be scaled by combining the outputs from many individual elements. However, the output of such diode arrays typically exhibits a very poor beam quality [2] or a relatively large spectral bandwidth [3]. Recently techniques have been developed based on seeding arrays of semiconductor optical amplifiers (SOAs) from a single laser, to generate output beams that can be combined coherently [4]. These coherent beam combination (CBC) diodes offer the potential for increasing the brightness of the output beam while maintaining a narrow spectrum bandwidth. However, for CBC diodes, previous reports have highlighted shortcomings such as diode system size, cost, and the requirement of complex optical architectures. Here we report a simple, scalable monolithically integrated system comprising a laterally-coupled 1.55 µm distributed feedback (DFB) laser feeding two stages of multi-mode interference couplers (MMIs) and SOAs to deliver high power beams with a quasi-single-spatial-mode far field pattern (FFP). Furthermore, compared with conventional buried-grating and selectively etched and re-grown techniques for

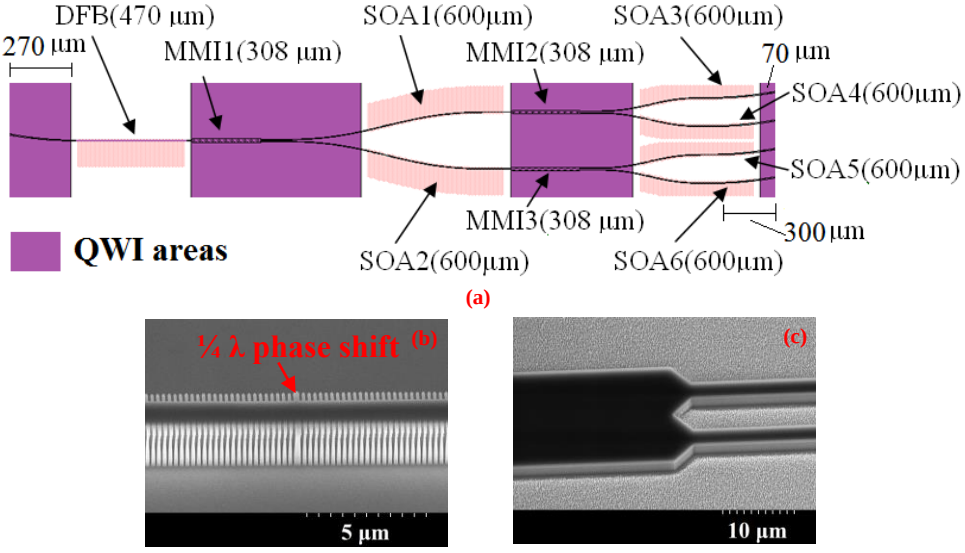

Fig.1. (a) Schematic of the device, (b) SEM picture of the first-order 50% duty cycle sidewall gratings with a 0.6 µm recess and λ/4 phase shift, (c) the MMI output side.

photonic integration, our technique of post-growth processing based on side-wall gratings and quantum-well intermixing (QWI), offers a simple, flexible and low-cost alternative.

The epitaxial structure and fabrication process used for the device are similar to those described in [5]. The schematic of the fabricated device along with its dimensions are shown in Fig. 1(a). The active components involved are a laterally coupled DFB laser [6] and six SOAs. The DFB laser has a cavity length (L) of 470 µm. The gratings are of first-order with a 50% duty cycle, formed by etching 0.6 µm recesses into the sidewalls of the waveguide, as shown in Fig. 1(b). The period of the grating is 244 nm. A λ/4 phase shift segment was positioned in the center of the DFB laser cavity to ensure single longitudinal mode oscillation. The measured coupling coefficient, κ, is ~42 cm^{-1}. The relatively low κ value, compared with the simulated value of 82 cm^{-1}, may be due to the reactive ion etching (RIE) lag in the horizontal and vertical direction which reduces the coupling strength.

The regions between the active components are passive (dark shading in Fig. 1(a)) and are bandgap widened using the QWI technique to provide a 100 nm blue-shift only in those areas [5, 7]. Active devices based on ridge waveguides often exhibit beam steering in the far field as a result of asymmetric current injection on either side of the ridge. By placing 70 µm long passive waveguides adjacent to the output facets of the SOAs numbered 3-6, such beam steering effects are considerably reduced and the beam stability is thus improved.

The MMIs are 16 µm wide and 308 µm long. The ridge waveguide width throughout the remainder of the device is 2.5 µm, other than the rear output of the DFB laser and the output of the four SOAs, i.e., SOAs 3-6, where the waveguide is curved and flared from 2.5 µm to 6 µm along a distance of 300 µm. The curvature radius is 1727.6 µm and the tilt is 10° at the output facet to minimize back-reflections. The separation between two adjacent output SOAs is 125 µm. Raised cosine designs were used for the S-bends and discontinuities in the radius of curvature were avoided to minimize mode-mismatch losses [8]. The MMI sections were designed to minimize back reflections into the laser (Fig. 1(c)), where a 45° tilt was used at each corner of the input waveguides and the output waveguide. Small deviations from the calculated device dimensions are therefore not critical since back reflections within the MMIs are not coupled back into the input waveguides, which otherwise might result in deterioration of the signal quality of the DFB laser [9].

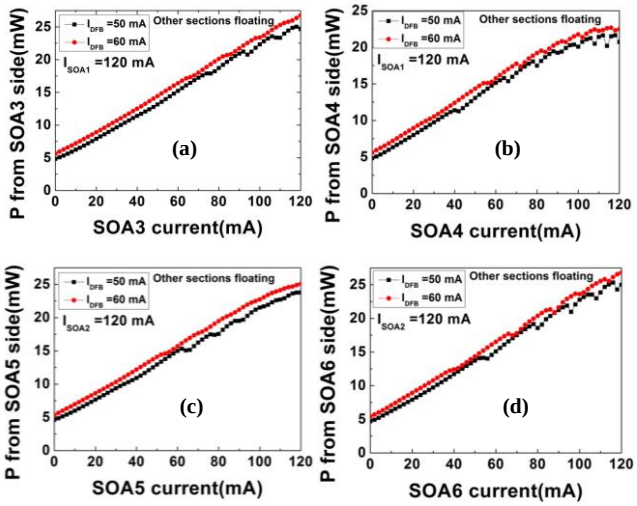

Fig.2. Measured output power from the second stage SOAs side vs $I_{SOA3\text{-}SOA6}$ when keeping I_{SOA1} =120 mA (a, b) and I_{SOA2} =120 mA (c, d) respectively.

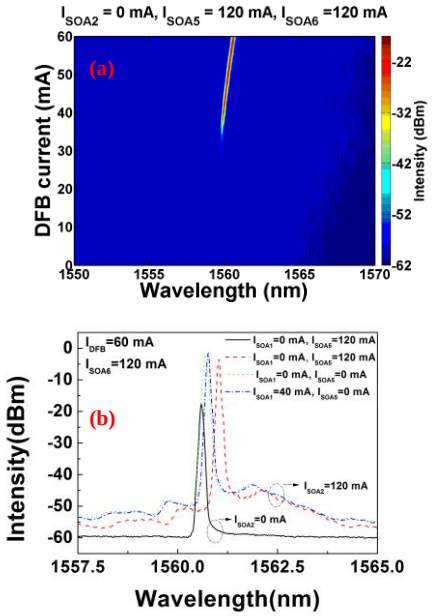

Fig.3. (a) 2-D optical spectra from SOA6 side as a function of I_{DFB} and (b) SOA6 side optical spectra when varying the current of SOA2, SOA1, and SOA5.

The threshold current of the DFB laser was measured to be 40 mA. The output powers (P) measured from SOA3 to SOA6 as a function of applied current are shown in Fig. 2, with I_{DFB} = 50, 60 mA, and the currents to SOA1 and SOA2, $I_{SOA1\text{-}2}$ = 120 mA. Some kinks were observed in the L-I curves, particularly around I_{DFB} = 50 mA, which are typical for a DFB laser and are caused by thermal detuning between the DFB and SOA sections. The maximum output power from each output at the SOA side was nearly the same, namely about 25 mW. This is indicative of the high quality of the 1×2 MMIs distributing the power evenly as expected. The measured total maximum output power was ~100 mW.

Figure 3(a) shows 2D optical spectra as a function of I_{DFB} from the SOA6 output facet when I_{SOA2} = 0 mA, I_{SOA5} = 120 mA, I_{SOA6} = 120 mA, with the other sections floating. We found the operation of the DFB laser was very stable with I_{SOA5} operating between 0 to 120 mA, confirming that the design of the MMI is effective in suppressing back-reflections (Fig. 1(c)). Figure 3(b) shows the spectra when I_{DFB} = 60 mA and I_{SOA6} =120 mA while varying the currents applied to SOA2, SOA1 and SOA5. When I_{SOA2} was increased from 0 mA to 120 mA, the amplified spontaneous emission (ASE) background noise increased but the side-mode suppression ratio (SMSR) remained almost unchanged at 42 dB. The peak wavelength was red-shifted from 1560.59 nm due to thermal effects. When increasing I_{SOA1} from 0 mA to 40 mA, the optical spectrum remained stable, which is again indicative of effective suppression of reflections from SOA1 to SOA2. When increasing I_{SOA5} from 0 mA to 120 mA, the peak wavelength was red-shifted due to the increased temperature of the device. Again, the SMSR was unchanged despite the wavelength shift. This confirms that the performance of the DFB laser was not compromised by the two-stage SOA operation, while the output power was increased. The optical spectra from SOAs 3-6 all have the same characteristics. Although we did not measure the combined optical spectrum, it will have the same characteristics as that measured from SOAs 3-6, albeit the peak position may be red shifted due to the total thermal loading when all of the output channels are driven simultaneously. It is anticipated that more effective heat-sinking combined with an improved temperature control feedback system will reduce thermal crosstalk between the components and improve the performance in terms of output power, wavelength stability, and degree of coherence of spatial beam combining.

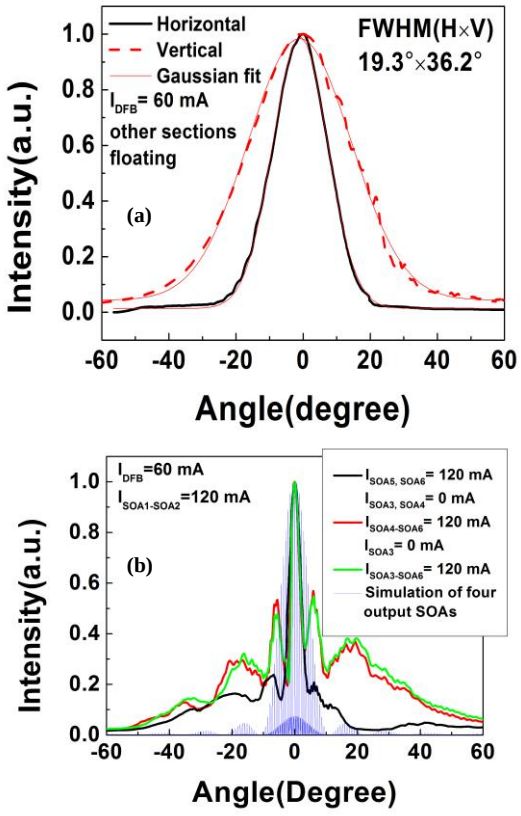

Fig.4. (a) measured FFP from the DFB laser side at I_{DFB} =60 mA and other sections floating, (b) measured in-plane FFP at I_{DFB} =60 mA, $I_{SOA1\text{-}SOA2}$ =120 mA, with two (black solid line), three (red line), four (green line) output SOAs pumped with an injection current of 120 mA and simulation (blue line) of four output SOAs using diffraction theory. Note the FFPs are offset by 32° because of the angled facet.

Fig. 4(a) shows the measured FFP from the DFB laser rear output facet under the operation condition of I_{DFB} = 60 mA with other sections floating. The full-width at half-maximum (FWHM) of the beam divergences were 19.3° × 36.2°. Compared with conventional laser diodes, the beam divergence angle was reduced by ~10° in the horizontal direction, due to the curved and flared rear output ridge waveguide (from 2.5 μm to 6 μm along a distance of 300 μm). This beam profile is highly desirable when coupling to a single-mode fiber, for instance. It should be noted that due to the 10° tilt angle of the SOA facet, there is a ~32° offset in the horizontal direction angle, which is consistent

with the calculated value of 32.4˚. Figure 4(b) shows the quasi-single spatial-mode FFP measured from the SOAs 3-6 output facets using I_{DFB} = 60 mA, $I_{SOA1\text{-}SOA2}$ = 120 mA, with two (SOA5 and SOA6, black solid line), three (SOA4-SOA6, red dash line), and four (SOA3-SOA6, green dot line) output SOAs simultaneously pumped, each with an injection current of 120 mA. Furthermore, we used diffraction theory to simulate the FFP when all four output SOAs are driven (blue line), and the envelope is similar to that of the measured results. It is evident that, by pumping more SOA output channels, the output power is increased and the main lobe divergence angle becomes narrower. The narrowest measured FFP was 3.5° FWHM at the central in-plane peak, which is significantly larger than the simulated value of 0.2°. The reason for this discrepancy is the resolution limit of the FFP measurement system is 0.9° FWHM. ASE from the SOAs decreases the temporal and spatial coherence, and its effect can been seen as raised pedestals in the experimental curves of Fig. 4(b). The power ratio in the main lobe represents 36%, 15%, and 14% for each of the three cases. The scalability of this approach is evident when comparing the FFPs, which maintained high coherence when combing two, three or four channels. Because SOA3 to SOA6 are fed from a single DFB laser, their output light is mutually coherent, and interference patterns at the output reflected this. In principle, the device architecture is highly scalable, i.e. the number of MMI and SOA stages could be increased, and the total output power would scale by 2^N, where N is the number of the stages of the MMIs and SOAs.

In summary, we have demonstrated a scalable monolithically integrated system comprising a laterally-coupled 1.55 μm DFB laser with two stages of MMIs and SOAs for delivering high power with a quasi-single spatial-mode FFP. A single DFB laser was used as a seed and about 100 mW output power with a low divergence angle of 3.5º in the central of in-plane peak was achieved with a bias current of 60 mA applied to the DFB and 120 mA to each of the SOAs. Stable single-frequency operation with a high SMSR (>40 dB) was maintained over a wide range of operating currents applied to the two-stage SOA sections. The device fabrication method, based on side-wall gratings and QWI, offers a simple, flexible and low cost alternative technique to conventional fabrication methods. These devices are expected to open up many applications for future compact high power 1.55 μm DFB lasers.

The authors would like to acknowledge the staff of the James Watt Nanofabrication Centre at the University of Glasgow for help in fabricating the devices reported in this paper. The authors also would like to thank Dr Marc Sorel and Mohsin Haji for their contributions to this work.

References

[1] S. R. Selmic, G. A. Evans, T. M. Chou, J. B. Kirk, J. N. Walpole, J. P. Donnelly, C. T. Harris, and L. J. Missaggia, IEEE Photon. Technol. Lett. **14**, 890-892 (2002).

[2] V. C. Elarde, K. E. Tobin, R. K. Price, V. B. Verma, and J. J. Coleman, IEEE Photon. Technol. Lett. **20**, 1085-1087 (2008).

[3] B. Chann, R. K. Huang, L. J. Missaggia, C. T. Harris, Z. L. Liau, A. K. Goyal, J. P. Donnelly, T. Y. Fan, A. Sanchez-Rubio, and G. W. Turner, Opt. Lett. 30, 2104 (2005).

[4] S. M. Redmond, K. J. Creedon, J. E. Kansky, S. J. Augst, L. J. Missaggia, M. K. Connors, R. K. Huang, B. Chann, T. Y. Fan, G. W. Turner, and A. S. Rubio, Opt. Lett. **36**, 999-1001 (2011)

[5] L. Hou, M. Haji, R. Dylewicz, B. C. Qiu, A. C. Bryce, IEEE Photon. Technol. Lett. **23**, 82 (2011).

[6] H. Abe, S. G. Ayling, J. H. Marsh, R. M. De La Rue, and J. S. Roberts, IEEE Photon. Technol. Lett. **7**, 452 (1995).

[7] S. D. McDougall, O. P. Kowalski, C. J. Hamilton, F. Camacho, B. Qiu, M. Ke, R. M. De La Rue, A. C. Bryce, and J. H. Marsh, IEEE J. Select. Topics Quantum Electron. **4**, 636 (1998).

[8] W. J. Minford, S. K. Korotky, and R. D. Alferness, IEEE J. Quantum Electron. **18,** 1802 (1982).

[9] R. Hanfoug, L. M. Augustin, Y. Barabarin, J. J. G. M. van der Tol, E. A. J. M. Bente, F. Karouta, D. Rogers, S. Cole, Y. S. Oei, X. J. M. Leijtens and M. K. Smit, Electron. Lett. **42**, 465 (2006).

References with titles

[1] S. R. Selmic, G. A. Evans, T. M. Chou, J. B. Kirk, J. N. Walpole, J. P. Donnelly, C. T. Harris, and L. J. Missaggia, "Single frequency 1550-nm AlGaInAs–InP tapered high-power laser with a distributed Bragg reflector", IEEE Photon. Technol. Lett. **14**, 890-892 (2002).

[2] V. C. Elarde, K. E. Tobin, R. K. Price, V. B. Verma, and J. J. Coleman, "Curved waveguide array diode lasers for high-brightness applications", IEEE Photon. Technol. Lett. **20**, 1085-1087 (2008).

[3] B. Chann, R. K. Huang, L. J. Missaggia, C. T. Harris, Z. L. Liau, A. K. Goyal, J. P. Donnelly, T. Y. Fan, A. Sanchez- Rubio, and G. W. Turner, "Near-diffraction-limited diode laser arrays by wavelength beam combining", Opt. Lett. 30, 2104 (2005)

[4] S. M. Redmond, K. J. Creedon, J. E. Kansky, S. J. Augst, L. J. Missaggia, M. K. Connors, R. K. Huang, B. Chann, T. Y. Fan, G. W. Turner, and A. S. Rubio, "Active coherent beam combining of diode lasers", Opt. Lett. **36**, 999-1001 (2011)

[5] L. Hou, M. Haji, R. Dylewicz, B. C. Qiu, A. C. Bryce, "10 GHz mode-locked extended cavity laser integrated with surface-etched DBR fabricated by Quantum Well Intermixing", IEEE Photon. Technol. Lett. **23**, 82 (2011).

[6] H. Abe, S. G. Ayling, J. H. Marsh, R. M. De La Rue, and J. S. Roberts, "Single-mode operation of a surface grating distributed feedback GaAs-AlGaAs laser with variable-width waveguide", IEEE Photon. Technol. Lett. **7**, 452 (1995).

[7] S. D. McDougall, O. P. Kowalski, C. J. Hamilton, F. Camacho, B. Qiu, M. Ke, R. M. De La Rue, A. C. Bryce, and J. H. Marsh, "Monolithic integration via a universal damage enhanced quantum-well intermixing technique," IEEE J. Select. Topics Quantum Electron. **4**, 636 (1998).

[8] W. J. Minford, S. K. Korotky, and R. D. Alferness, "Low-loss Ti: Li NbO_3 waveguide bends at λ= 1.3 μm", IEEE J. Quantum Electron. **18,** 1802 (1982).

[9] R. Hanfoug, L. M. Augustin, Y. Barabarin, J. J. G. M. van der Tol, E. A. J. M. Bente, F. Karouta, D. Rogers, S. Cole, Y. S. Oei, X. J. M. Leijtens and M. K. Smit, "Reduced reflections from multimode interference couplers", Electron. Lett. **42**, 465 (2006).